

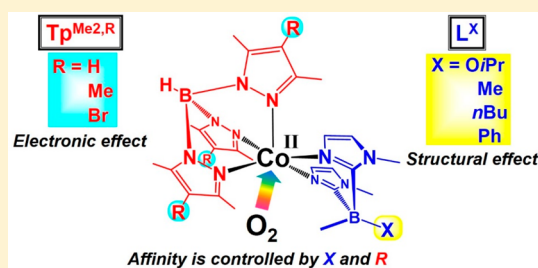
## Tuning the O<sub>2</sub> Binding Affinity of Cobalt(II) Centers by Changing the Structural and Electronic Properties of the Distal Substituents on Azole-Based Chelating Ligands

 Toshiki Nishiura, Yosuke Chiba, Jun Nakazawa,\*<sup>1</sup> and Shiro Hikichi\*<sup>2</sup>

Department of Material and Life Chemistry, Faculty of Engineering, Kanagawa University 3-27-1 Rokkakubashi, Kanagawa-ku, Yokohama 221-8686, Japan

### Supporting Information

**ABSTRACT:** The effects of the substituents on the chelating ligands located in the secondary coordination sphere on the O<sub>2</sub> affinity of cobalt(II) centers have been explored. The combination of facially capping tridentate tris(pyrazolyl)borates (= Tp<sup>Me2,4R</sup>) and bidentate bis(imidazolyl)borates (= [B(Im<sup>N-Me</sup>)<sub>2</sub>MeX]<sup>-</sup>; L<sup>X</sup>) yields square-pyramidal cobalt(II) complexes. The structural properties of the substituent groups X attached to the boron center of L<sup>X</sup> affect the arrangement of X in the resulting cobalt(II) complexes [Co<sup>II</sup>(Tp<sup>Me2,4R</sup>)(L<sup>X</sup>)]. When the boron-attached moiety of X is a relatively bulky sp<sup>3</sup>-CH<sub>2</sub>Y group (i.e., X:Y = Me:H and *n*Bu:*n*Pr), the alkyl group X faces the cobalt center, whereas for isopropoxy (OiPr) and phenyl (Ph) groups, of which the boron-attached atoms are a less hindered oxygen atom and a planer sp<sup>2</sup>-carbon, respectively, the X group is arranged away from the cobalt center. This flexible behavior of L<sup>X</sup> is reflected in the O<sub>2</sub> affinity of the cobalt(II) center, which depends on the extent to which the complex sphere is shielded by the ligands. The dependence of the cobalt(II) oxidation potential on the X substituent of L<sup>X</sup> is inconsistent with the O<sub>2</sub> affinity. On the other hand, the electronic properties of R, which is attached to the fourth position of the pyrazolyl rings in the rigid Tp<sup>Me2,4R</sup> ligand, are reflected in the electrochemical properties and O<sub>2</sub> affinity of the cobalt center.



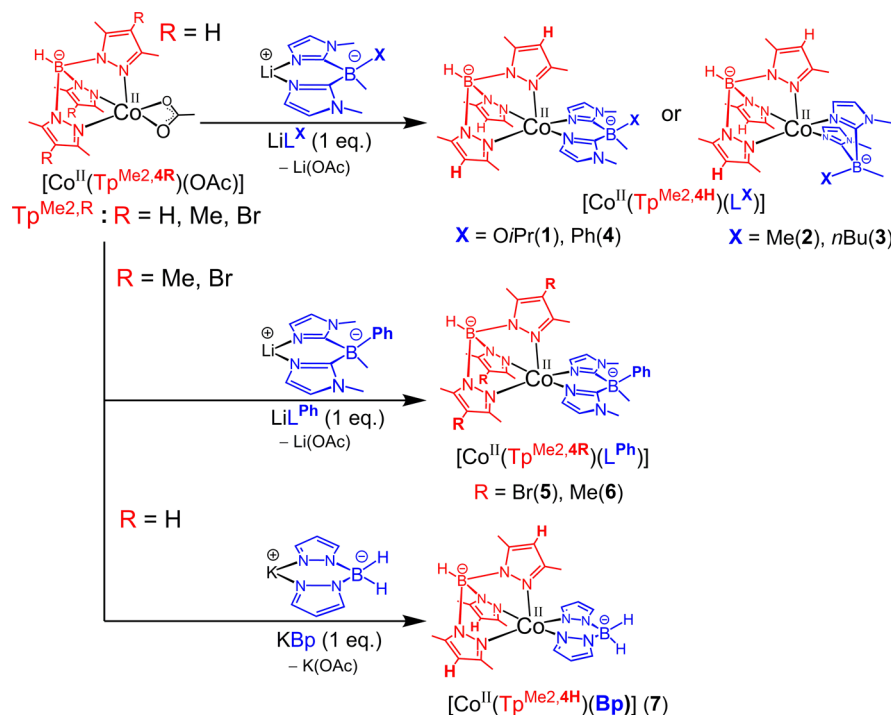
### 1. INTRODUCTION

In enzymes that catalyze oxidation reactions and respiratory pigments that function as O<sub>2</sub> carriers in living systems, dioxygen complexes of transition metals are formed via oxidative addition of the dioxygen molecule to a coordinatively unsaturated metal center.<sup>1–3</sup> Therefore, investigations of transition-metal complexes that exhibit an O<sub>2</sub> binding ability that mimics the functions of living systems have been of continuous interest because these investigations provide useful information for understanding O<sub>2</sub> metabolic processes and for constructing functional materials, such as catalysts, gas absorbents, and permeation agents.<sup>4–6</sup> Controlling the O<sub>2</sub> affinity of the metal center by tuning the coordination environment is a promising approach for obtaining highly efficient materials. The dioxygen-binding metal centers in biological O<sub>2</sub> transport systems are supported by azole-based ligands such as a porphyrin (polypyrrrole) and a histidine residue (imidazole). In hemoglobin/myoglobin, which are mammalian O<sub>2</sub> transport and storage heme proteins, mononuclear iron centers are supported by five azoles composed of an equatorial tetracyclic porphyrin and an axial imidazole.<sup>7</sup> In contrast, nonheme O<sub>2</sub> transport proteins, namely, hemocyanin and hemerythrin, involve dinuclear metal centers supported by terminal imidazole ligands. O<sub>2</sub> is trapped between two copper(I) centers in hemocyanin,<sup>8</sup> whereas in hemerythrin, one of two iron(II) centers, which is supported by an N2O3 donor set, captures O<sub>2</sub>.<sup>9</sup>

We have designed O<sub>2</sub>-binding mononuclear nonheme metal complexes involving “five azole-supported” transition-metal centers<sup>10</sup> by combining facially capping tridentate N3 donors, hydrotris(3,4,5-substituted-1-pyrazolyl)borates (= [HB(pz<sup>R</sup>)<sub>3</sub>]<sup>-</sup>; Tp<sup>R</sup>),<sup>11,12</sup> with bidentate N2 donors, bis(1-methyl-2-imidazolyl)borates (= [B(Im<sup>N-Me</sup>)<sub>2</sub>MeX]<sup>-</sup>; L<sup>X</sup>).<sup>13–20</sup> These chelating reagents act as monoanionic ligands composed of tetra-coordinated boron centers and azoles. Both ligands have great advantages for controlling the steric and electronic properties of the resulting metal complexes. In the metal complexes of Tp<sup>R</sup>, the properties of the substituent groups (= R<sup>3</sup>, R<sup>4</sup>, and R<sup>5</sup>) on the pyrazolyl rings of Tp<sup>R</sup> affect the nature of the metal centers. Interestingly, the substituent at the R<sup>4</sup> site of the pyrazolyl ring, which is positioned distal to the metal center, affects the electronic nature without changing the steric environment of the metal center.<sup>11,12,21</sup> In the case of L<sup>X</sup>, the boron-attached group X affects the dihedral angle of the two imidazolyl rings as well as the arrangement of another boron-attached methyl group.<sup>17</sup> In this study, we have explored the effects of the ligand substituent groups located in the secondary coordination sphere (i.e., R of hydrotris(3,5-dimethyl-4-R-pyrazolyl)borates (Tp<sup>Me2,4R</sup>) and X of L<sup>X</sup>) on the O<sub>2</sub> affinity of the supported transition-metal centers. We chose cobalt as the central metal because the dioxygen

Received: August 8, 2018

Scheme 1. Synthesis of Co(II) Complexes



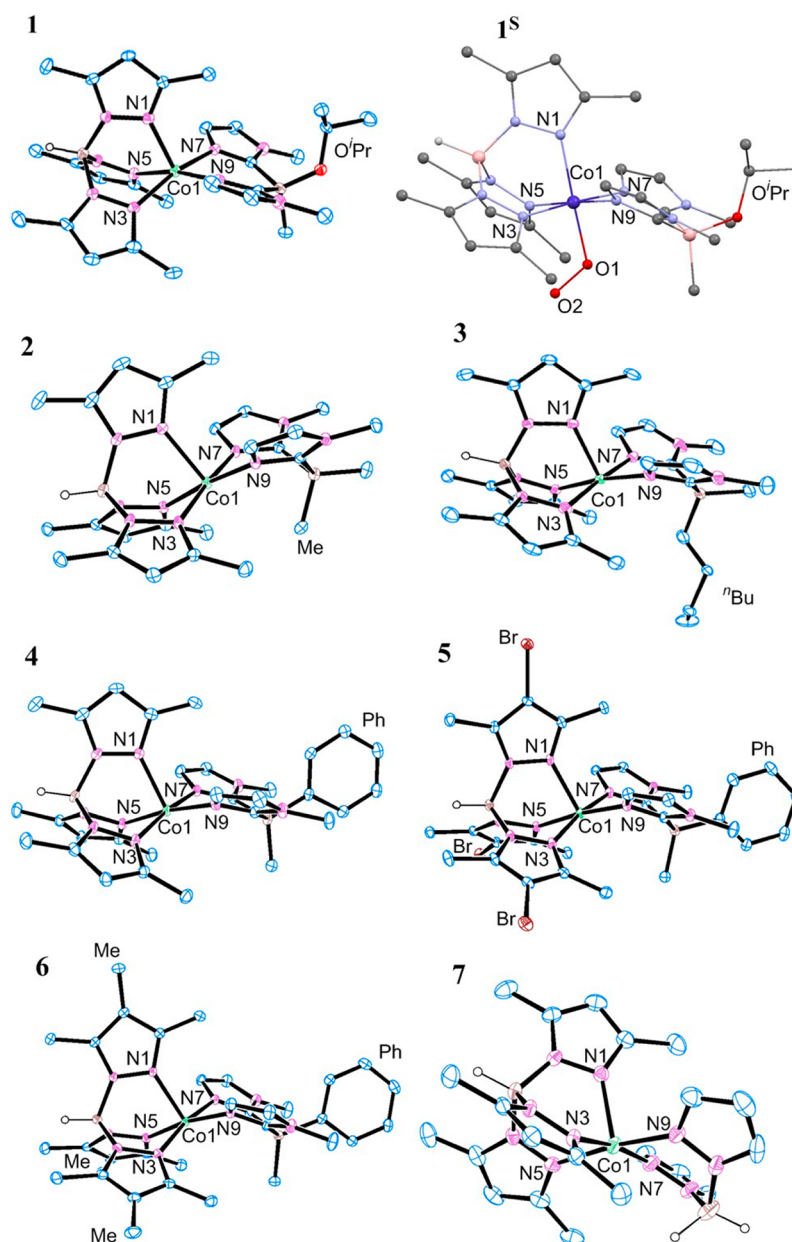
complexation chemistry of cobalt(III) species is well established,<sup>22–26</sup> and interest in cobalt-O<sub>2</sub> compounds from the viewpoints of bioinorganic<sup>27–44</sup> to material<sup>45–59</sup> chemistry has been growing. In addition, cobalt complexes are generally robust against irreversible oxidative transformations, unlike the related iron analog.<sup>60–62</sup> Therefore, the study of cobalt complexes would facilitate examination of the effects of the ligands.

## 2. RESULTS AND DISCUSSION

**2.1. Structural Characterization of Mixed Ligand Complexes.** In this study, we investigated a series of mixed ligand complexes of cobalt(II),  $[\text{Co}^{\text{II}}(\text{Tp}^{\text{Me2,4R}})(\text{L}^{\text{X}})]$  (1–6; see Scheme 1) and a related complex  $[\text{Co}^{\text{II}}(\text{Tp}^{\text{Me2,4H}})(\text{Bp})]$  (7; Bp denotes dihydrobis(pyrazolyl)borate). The mixed ligand complexes were synthesized by the reaction of acetato complexes  $[\text{Co}^{\text{II}}(\text{Tp}^{\text{Me2,4R}})(\kappa^2\text{-OAc})]$ <sup>63</sup> with alkaline metal salts of the bidentate azole ligands  $\text{LiL}^{\text{X}}$  and KBp. The molecular structures of all the synthesized cobalt(II) complexes were revealed by X-ray crystallography and are summarized in Figure 1 and Table 1.

**2.1.1. Coordination Properties of  $\text{L}^{\text{X}}$  in the  $\text{Tp}^{\text{Me2,4H}}$  Complexes.** The coordination structures of the cobalt(II) centers in 1–4 are very similar to each other: The square-pyramidal cobalt(II) centers are supported by three pyrazolyl nitrogens of  $\text{Tp}^{\text{Me2,4H}}$  and two imidazolyl nitrogens of  $\text{L}^{\text{X}}$  (1–4 in Figure 1). Interestingly, the arrangement of X bound to the boron center can be categorized into two groups depending on the structural properties of X. When X = Me and *n*Bu, within which the boron-attached  $\alpha$ -carbon is a relatively bulky  $\text{sp}^3$ -CH<sub>2</sub>Y group (Y = H and *n*Pr), the alkyl groups approach the cobalt centers in 2 and 3. In contrast, the isopropoxy (OiPr) and phenyl (Ph) groups, within which the boron-attached atoms are a less hindered oxygen atom and a planer  $\text{sp}^2$ -carbon, respectively, are located away from the cobalt centers in 1 and 4. As a result, a large amount of space exists around the sixth

vacant site on the cobalt center in 1 and 4, whereas the space around the sixth vacant site on 2 and 3 is more narrow because the Me and *n*Bu groups face the metal center. To quantitatively assess the structural effects of X on 1–4, the percentage of the complex sphere shielded by the ligands was calculated based on solid angle analyses.<sup>64</sup> Complexes 2 and 3 containing  $\text{L}^{\text{Me}}$  and  $\text{L}^{\text{nBu}}$  showed sphere-shielding percentages of 94.0% and 94.6%, respectively. In contrast, the corresponding values for 1 ( $\text{L}^{\text{OiPr}}$ ) and 4 ( $\text{L}^{\text{Ph}}$ ) were 89.9 and 91.3%, respectively (see drawings of the sphere-shielding and space filling diagrams provided as Figures S8 and S9 in Supporting Information). Similar trends in the arrangement of X have been observed for  $[\text{Ni}(\text{L}^{\text{X}})_2]$  (where X = OMe, H, Me, *n*Bu, and Ph) and  $[\text{Ni}^{\text{II}}(\text{Tp}^{\text{iPr2}})(\text{L}^{\text{X}})]$  complexes ( $\text{Tp}^{\text{iPr2}}$  = hydrotris(3,5-diisopropyl-1-pyrazolyl)borate and X = Me and *n*Bu).<sup>17</sup> The observed trend in the orientation of the boron-attached X groups has been attributed to the steric interactions around both the boron center of  $\text{L}^{\text{X}}$  and the metal center of the resulting complex. In both previous homoleptic nickel complexes  $[\text{Ni}(\text{L}^{\text{X}})_2]$  and the presented heteroleptic cobalt complexes  $[\text{Co}^{\text{II}}(\text{Tp}^{\text{Me2,4H}})(\text{L}^{\text{X}})]$ , the bulkiness of the boron-attached part of X affects the dihedral angles between two imidazolyl rings of  $\text{L}^{\text{X}}$ . When X is Me or *n*Bu, two 1-methyl groups on the imidazolyl rings and the boron-attached methyl group of  $\text{L}^{\text{X}}$  are oriented to the opposite site of the metal center, and the steric repulsion between these methyl groups leads the smaller dihedral angles (in  $[\text{Ni}(\text{L}^{\text{X}})_2]$ : 118.6° (X = Me) and 123.6° (X = *n*Bu),<sup>17</sup> in  $[\text{Co}^{\text{II}}(\text{Tp}^{\text{Me2,4H}})(\text{L}^{\text{X}})]$ : 123.5° (X = Me; 2) and 129.6° (X = *n*Bu; 3)) as well as approaching of X to the metal center due to tetrahedral borate geometry. In contrast, the planar phenyl group and the less sterically demanding oxygen atom of the alkoxide groups are located in the cleft formed by two 1-methyl groups on  $\text{L}^{\text{Ph}}$  and  $\text{L}^{\text{OR}}$ , and those result in the larger dihedral angles on two imidazolyl rings (in  $[\text{Ni}(\text{L}^{\text{X}})_2]$ : 129.2° (X = Ph) and 125.6° (X = OMe),<sup>17</sup> in  $[\text{Co}^{\text{II}}(\text{Tp}^{\text{Me2,4H}})(\text{L}^{\text{X}})]$ : 144.6° (X = Ph; 4) and

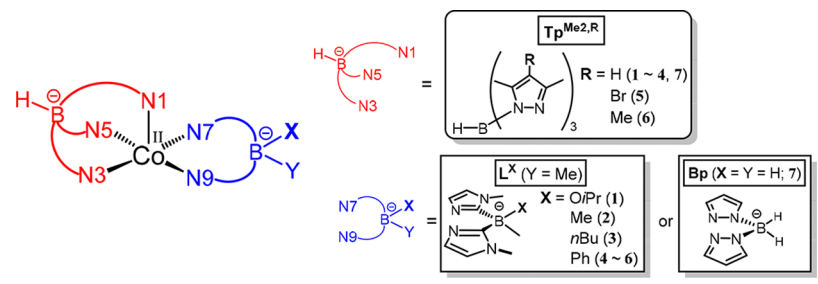


**Figure 1.** ORTEP diagrams of  $[\text{Co}^{\text{II}}(\text{Tp}^{\text{Me2,4R}})(\text{L}^{\text{X}})]$  (**1–6**) and  $[\text{Co}^{\text{II}}(\text{Tp}^{\text{Me2,4H}})(\text{Bp})]$  (**7**) and a ball and stick drawing of  $[\text{Co}^{\text{III}}(\text{O}_2^-)(\text{Tp}^{\text{Me2,4H}})(\text{L}^{\text{O}i\text{Pr}})]$  (**1<sup>S</sup>**). All hydrogen atoms are omitted for clarity; ellipsoids are set at 30% probability.

156.4° ( $X = \text{O}i\text{Pr}$ ; **1**), and the boron-attached methyl group in these complexes is arranged away from the metal center. Notably, difference in the amplitude of the dihedral angles between  $\text{L}^{\text{alkyl}}$  (**2** and **3**) and others ( $\text{L}^{\text{Ph}}$  and  $\text{L}^{\text{O}i\text{Pr}}$ ; **4** and **1**) in  $[\text{Co}^{\text{II}}(\text{Tp}^{\text{Me2,4H}})(\text{L}^{\text{X}})]$  is larger than that observed in  $[\text{Ni}(\text{L}^{\text{X}})_2]$ . In the entitled cobalt complexes **1–4**, the cobalt centers are surrounded by three methyl groups attached on the R<sup>3</sup> position of the pyrazolyl rings of  $\text{Tp}^{\text{Me2,4H}}$ , and steric repulsion between these methyl groups and the C–H groups of fourth position of imidazolyl rings seems to affect the dihedral angles of  $\text{L}^{\text{X}}$ . In the  $\text{L}^{\text{alkyl}}$  complexes of nickel with the bulky  $\text{Tp}^{\text{iPr2}}$ ,  $[\text{Ni}^{\text{II}}(\text{Tp}^{\text{iPr2}})(\text{L}^{\text{X}})]$ , however, the steric repulsion between the metal-surrounding *iPr* groups and the boron-bounded alkyl groups is critical to the amplitude of the dihedral angles of  $\text{L}^{\text{alkyl}}$ , as found in the difference of the dihedral angles 129.9° ( $X = \text{Me}$ ) vs 160.3° ( $X = n\text{Bu}$ ).<sup>17</sup>

**2.1.2. Effect of R on  $\text{Tp}^{\text{Me2,4R}}$ .** Then, we examined the effects of R on  $\text{Tp}^{\text{Me2,4R}}$  by introducing an electron-donating methyl (Me) or electron-withdrawing bromine (Br) group as the substituent (= R) at the fourth position of the pyrazoles.  $\text{L}^{\text{Ph}}$  was employed as a bidentate partner because its cobalt(III)-superoxo derivative was the most stable in a series of  $\text{Tp}^{\text{Me2,4H}}$  complexes, as will be shown later. As we expected, the molecular structures of the  $\text{Tp}^{\text{Me2,4Br}}$  (**5**) and  $\text{Tp}^{\text{Me2,4Me}}$  (**6**) derivatives were very similar to that of the  $\text{Tp}^{\text{Me2,4H}}$  complex (**4**). In particular, identical arrangements of the phenyl group in  $\text{L}^{\text{Ph}}$  were observed for complexes **4**, **5**, and **6**.

**2.1.3. Bp Complex.** To clarify the effects of the steric and electronic properties of the bidentate ligands, an analogous mixed ligand complex  $[\text{Co}^{\text{II}}(\text{Tp}^{\text{Me2,4H}})(\text{Bp})]$  (**7**; where Bp = dihydrobis(pyrazolyl)borate) was also investigated. The whole molecular structure of the cobalt(II) complex **7** was similar to those of complexes **1–4** with  $\text{L}^{\text{X}}$  derivatives and previously

Table 1. Structural Parameters of 1–7 and 1<sup>Sa</sup>


	1	1 <sup>Sb</sup>	2	3	4	5	6	7
Bond Lengths (Å)								
Co1-N1	2.107(3)	2.052(4)	2.115(3)	2.117(7)	2.119(2)	2.102(2)	2.092(3)	2.096(3)
Co1-N3	2.057(3)	1.978(3)	1.974(2)	1.959(7)	1.965(2)	1.974(2)	1.967(2)	1.986(2)
Co1-N5	2.044(3)	2.005(4)	1.974(2)	1.975(7)	1.965(2)	1.966(2)	1.967(2)	2.015(2)
Co1-N7	1.996(3)	1.962(4)	1.937(2)	1.922(7)	1.923(2)	1.919(2)	1.928(2)	1.990(2)
Co1-N9	1.971(3)	1.952(3)	1.937(2)	1.941(7)	1.923(2)	1.922(2)	1.928(2)	1.975(2)
Co1-O1	—	1.901(3)	—	—	—	—	—	—
O1-O2	—	1.301(5)	—	—	—	—	—	—
Selected Angles (°)								
N1-Co1-N3	89.3(1)	89.9(2)	90.8(1)	90.7(3)	91.4(1)	90.5(1)	91.2(1)	90.8(1)
N1-Co1-N5	92.2(1)	90.8(2)	90.8(1)	91.6(3)	91.4(1)	90.2(1)	91.2(1)	90.6(1)
N1-Co1-N7	103.6(1)	93.2(2)	94.4(1)	94.1(3)	95.9(1)	98.1(1)	98.4(1)	99.0(1)
N1-Co1-N9	97.7(1)	90.6(2)	94.4(1)	95.1(3)	95.9(1)	96.3(1)	98.4(1)	96.8(1)
N3-Co1-N5	82.3(1)	88.4(2)	87.6(1)	87.1(3)	86.3(1)	88.4(1)	87.3(1)	86.5(1)
N3-Co1-N7	166.7(1)	176.8(2)	174.7(1)	175.0(3)	172.6(1)	171.4(1)	170.4(1)	170.3(1)
N3-Co1-N9	91.9(1)	91.3(2)	91.1(1)	92.9(3)	92.2(1)	90.8(1)	91.6(1)	90.4(1)
N5-Co1-N7	93.8(1)	91.4(2)	91.1(1)	91.3(3)	92.2(1)	92.0(1)	91.6(1)	92.9(1)
N5-Co1-N9	168.5(1)	178.5(2)	174.7(1)	173.2(3)	172.6(1)	173.5(1)	170.4(1)	172.0(1)
N7-Co1-N9	89.6(1)	88.8(2)	89.7(1)	88.1(3)	88.4(1)	87.9(1)	87.9(1)	88.9(1)
Co-O1-O2	—	119.6(3)	—	—	—	—	—	—
dihedral angles of L <sup>X</sup> (°)	156.41	146.82	123.54	129.63	144.64	137.08	144.49	117.75 <sup>d</sup>
τ <sup>c</sup>	0.03	0.03	0	0.03	0	0.04	0	0.03

<sup>a</sup>Due to the presence of a mirror plane (on Co1-N1-B1), the atom numberings N5, N7, and N9 of complexes 2, 4, and 6 in this table correspond to the N3', N5, and N5' atoms, respectively, in the crystallographic data. <sup>b</sup>From ref 10. <sup>c</sup>(The largest angle – the second-largest angle)/60°. <sup>d</sup>Dihedral angle of Bp.

reported Tp<sup>R</sup>-Bp<sup>R</sup> mixed ligand complexes.<sup>65,66</sup> A τ value of 0.03 indicated that the cobalt center of 7 had a slightly distorted square-pyramidal geometry. The dihedral angle between the two pyrazoles of Bp in 7 was 125.0°, and one of two hydrogen atoms attached to the boron center of Bp was pointed toward the cobalt center. However, the distance from the hydrogen atom to the cobalt center was 3.02 Å, and a large open space surrounded the sixth vacant site on the cobalt center. In fact, solid angle analysis revealed that the percentage of the sphere shielded by the ligands was 90.5%, which was comparable to the values for the L<sup>O<sup>i</sup>Pr</sup> and L<sup>Ph</sup> complexes 1 and 4.

**2.1.4. Cobalt(III)-Superoxo Complex 1<sup>S</sup>.** The molecular structure of an O<sub>2</sub> adduct of 1 was determined, as reported in the earlier communication.<sup>10</sup> An O–O bond length of 1.301(5) Å is typical for a superoxide ligand. The IR spectrum of this O<sub>2</sub> adduct in the solution state exhibited an O–O bond stretching vibration at 1147 cm<sup>-1</sup> for the <sup>16</sup>O<sub>2</sub> derivative and at 1088 cm<sup>-1</sup> for the <sup>18</sup>O<sub>2</sub> derivative. Additionally, the EPR spectrum (measured at –198 °C) showed a signal at approximately *g* = 2 with eight-line hyperfine coupling. These spectroscopic properties are consistent with the assignment of the O<sub>2</sub> adduct of 1 as an end-on superoxide complex of mononuclear low-spin cobalt(III), [Co<sup>III</sup>(O<sub>2</sub><sup>-</sup>)(Tp<sup>Me2,4H</sup>)(L<sup>O<sup>i</sup>Pr</sup>)] (1<sup>S</sup>).

The superoxide ligand sits in a cleft between the two methyl groups of Tp<sup>Me2,4H</sup>, and the distal oxygen atom is pointed away from the boron-attached methyl group of L<sup>O<sup>i</sup>Pr</sup>. The Co–N bond lengths are 1.952(4)–2.052(4) Å, which are somewhat shorter than the corresponding lengths in the cobalt(II) precursor 1. Although shrinkage of the bond lengths between the cobalt center and the N-donor ligands occurs, the structure of the [Co(Tp<sup>Me2,4H</sup>)(L<sup>O<sup>i</sup>Pr</sup>)]<sup>+</sup> moiety of 1<sup>S</sup> is almost the same as that of 1. The boron-attached O<sup>i</sup>Pr group is arranged away from the cobalt(III) center in 1<sup>S</sup>, and the dihedral angle between the two imidazolyl rings of L<sup>O<sup>i</sup>Pr</sup> in 1<sup>S</sup> is 146.8°, whereas that in the precursor compound 1 is 156.4°. Solid angle analysis indicated that the percentage of the sphere shielded was 99.3% for the superoxide-bound state of 1<sup>S</sup> and 89.3% for the superoxide ligand-removed [Co(Tp<sup>Me2,4H</sup>)(L<sup>O<sup>i</sup>Pr</sup>)]<sup>+</sup> moiety of 1<sup>S</sup>, respectively. The latter value was very close to that observed for 1. Therefore, the coordination environment of the cobalt center seems to be retained during the oxygenation process.

In order to check the retention of the structures of the solid state superoxo complex in solution, DR-UV–vis spectra of the solid-state superoxo species and its precursor were measured. We could not measure the spectra of the solid-state superoxo species 1<sup>S</sup>–5<sup>S</sup> and 7<sup>S</sup> because of their lower thermal stabilities. In contrast, the solid-state superoxo species 6<sup>S</sup>, which was



obtained as dark brown precipitates by cooling the solution of  $6^S$  at  $-80\text{ }^\circ\text{C}$ , was suitable to measure the spectrum at ambient temperature and exhibited absorption bands around 400 and 530 nm. These absorption bands are similar to those observed in the spectrum of the solution of  $6^S$  (Figure S10).

**2.2. Elucidation of the Factors That Control the  $\text{O}_2$  Affinity.** As described above, the  $\text{L}^{\text{OiPr}}$  complex **1** reacted with  $\text{O}_2$  to give the corresponding end-on cobalt(III)-superoxo complex  $1^S$ . The other  $\text{L}^X$  complexes **2–6** also reacted with  $\text{O}_2$  at low temperature to give the corresponding cobalt(III)-superoxo complexes  $2^S\text{--}6^S$ , as evidenced by the similarity in the UV-vis spectra (Figure 2). All complexes exhibited two

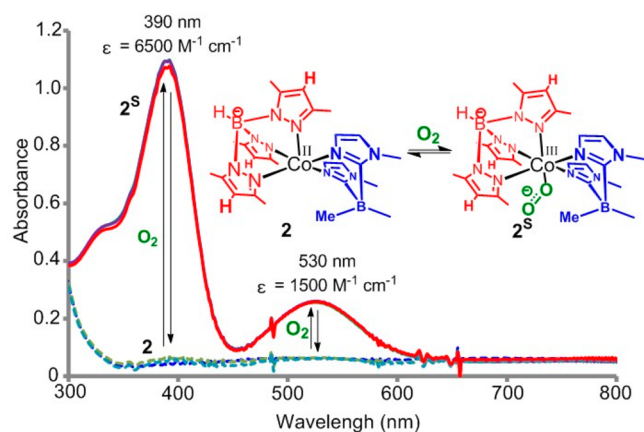


**Figure 2.** UV-vis spectral changes that occur during the reversible binding and release of  $\text{O}_2$  to **2** (0.16 mM in THF) at  $-80\text{ }^\circ\text{C}$ . Solid lines:  $\text{O}_2$  atmosphere, dashed lines: Ar atmosphere (removal of  $\text{O}_2$  by bubbling Ar through the solution of  $2^S$ ). To confirm the reversibility, bubbling of Ar and the following introduction of  $\text{O}_2$  were repeated twice to the solution after the recording of the first set (blue dashed spectrum; cobalt(II) complex under Ar, green spectrum: generated cobalt(III)-superoxo species by the reaction with  $\text{O}_2$ ). Colors of spectra mean as follows. Gray (dashed): first recovered cobalt(II) compound, purple: second generated superoxo species, pale blue (dashed): second recovered cobalt(II) compound, red: third generated superoxo species.

intense bands at approximately 390 and 530 nm, which are attributed to  $\text{O}_2^-$  to cobalt(III) charge transfer (CT) (Figures S11–S15). Repeated  $\text{O}_2$  and Ar bubbling of the solutions of **1–6** at an appropriate temperature led to reversible changes in the UV-vis spectra that corresponded to the addition and

dissociation of  $\text{O}_2$  to the cobalt centers. IR spectra of the  $\text{CH}_2\text{Cl}_2$  solutions of *in situ* generated  $2^S\text{--}6^S$  (measured at  $-80\text{ }^\circ\text{C}$ ; Figure S-17) exhibited vibrational bands around  $1150\text{ cm}^{-1}$  as found for  $1^S$  ( $1147\text{ cm}^{-1}$ ; described above). The Bp complex **7** also exhibited a similar reversible  $\text{O}_2$ -binding ability as found for **1–6** (Figure S16). Therefore, the thermodynamics of cobalt(II) oxygenation in complexes **1–7** were analyzed. As described below, the  $\text{O}_2$  affinity of the cobalt(II) centers, which were supported by the common  $3\text{N} + 2\text{N}$  scaffold, depended on the combination of  $\text{L}^X$  and  $\text{Tp}^{\text{Me}_2,4\text{R}}$ .

**2.2.1. Effects of the Electronic and Structural Properties of  $\text{L}^X$ .** The effect of X on  $\text{L}^X$  was examined by using  $\text{Tp}^{\text{Me}_2,4\text{H}}$  complexes **1–4** having different  $\text{L}^X$  ligands. A comparison of the temperature-dependent relative absorption intensities of the  $\text{O}_2$ -saturated solutions at 390 nm demonstrated that the order of thermal stability of the superoxo complexes was  $4^S$  (X = Ph) >  $1^S$  (OiPr) >  $2^S$  (Me) >  $3^S$  (*n*Bu) (Figure 3a). This order was quantitatively confirmed by the oxygen-binding equilibrium constants ( $= K_{\text{O}_2}$ ) determined by Drago's method,<sup>67</sup> in which the change in absorbance at 390 nm depended upon the partial pressure of oxygen supplied (Figure 4a and Table 2). The order of the  $K_{\text{O}_2}$  values determined at  $-50\text{ }^\circ\text{C}$  was not consistent with the order of the cobalt(II)/cobalt(III) oxidation potentials of **1–4**. The order of the oxidation potentials was **2** (0.07 V; X = Me) < **3** (0.12 V; *n*Bu) < **4** (0.18 V; Ph) < **1** (0.21 V; OiPr), which indicated that the distal substituent group X affected the electronic nature of the cobalt center (Figure 3b). On the other hand, the order of the  $K_{\text{O}_2}$  values seemed to be correlated with the percentage of the complex sphere shielded in the corresponding cobalt(II) precursors (see above). When X = Me or *n*Bu, the substituent faced the cobalt center, which led to a reduced  $\text{O}_2$  affinity (Figure 5).

The thermodynamic parameters of the oxygenation process obtained from van't Hoff plots (Figure 4b) indicated that the  $\Delta H$  values for **3** ( $-28.0\text{ kJ mol}^{-1}$ ) and **2** ( $-31.6$ ) were less favorable than those for **1** ( $-43.7$ ) and **4** ( $-59.8$ ), as summarized in Table 2. The entropy changes ( $= \Delta S$ ) for **2** ( $-134.0\text{ J mol}^{-1}\text{ K}^{-1}$ ) and **3** ( $-127.6$ ) were more positive (thermodynamically favorable) than those for **1** ( $-179.0$ ) and **4** ( $-243.5$ ), as shown in Table 2. As estimated from the crystallographic analysis of  $1^S$ , no significant structural changes occurred during the oxygenation process. Therefore, the

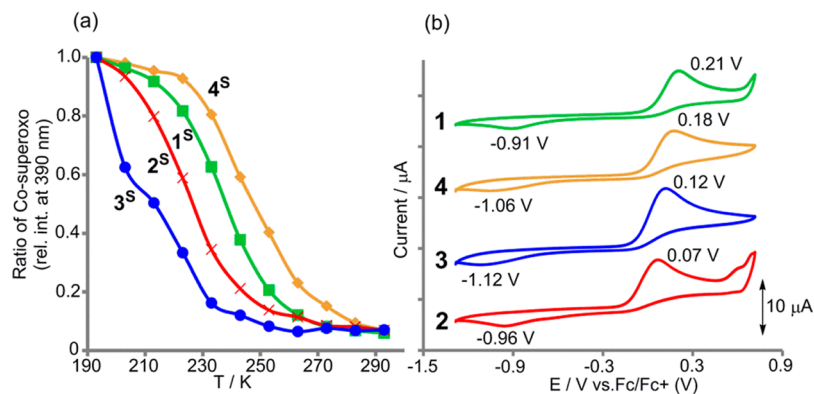


**Figure 3.** (a) Thermal stability of  $1^S\text{--}4^S$  in THF with a complex concentration of 0.16 mM and (b) cyclic voltammograms of **1–4** in  $\text{CH}_2\text{Cl}_2$  with 0.1 M  $\text{nBu}_4\text{NPF}_6$ .

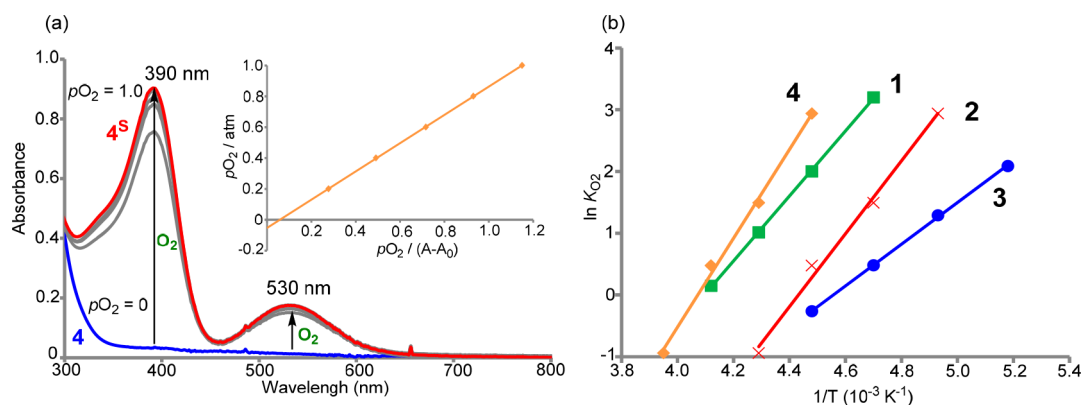


**Figure 4.** (a) Spectral changes of **4** under various  $O_2$  partial pressures ( $= p(O_2)$ ) in THF at  $-50\text{ }^\circ\text{C}$ .  $p(O_2) = 0, 0.2, 0.4, 0.6, 0.8,$  and  $1.0$  atm starting from the bottom. The initial spectrum of **4** ( $p(O_2) = 0$  atm) is shown in the blue line and the final saturated spectrum when  $p(O_2) = 1.0$  atm is the red line. The inset shows a plot of  $p(O_2)$  vs  $p(O_2)/(A - A_0)$  at  $390$  nm. (b) van't Hoff plots for the oxygenation of cobalt(II) complexes **1–4**.

**Table 2.** Equilibrium Constants ( $K_{O_2}$ ; measured at  $-50\text{ }^\circ\text{C}$ ) and Thermodynamic Parameters of **1–6**

complex	$K_{O_2}$ at $-50\text{ }^\circ\text{C}$ ( $\text{atm}^{-1}$ )	$\Delta S$ ( $\text{J}\cdot\text{K}^{-1}\cdot\text{mol}^{-1}$ )	$\Delta H$ ( $\text{kJ}\cdot\text{mol}^{-1}$ )	$\Delta G$ at $-50\text{ }^\circ\text{C}$ ( $\text{kJ}\cdot\text{mol}^{-1}$ )
<b>1</b>	7.40	$-179.0$ (21)	$-43.71$ (5)	$-3.71$
<b>2</b>	2.62	$-134.0$ (66)	$-31.58$ (14)	$-1.78$
<b>3</b>	0.77	$-127.6$ (18)	$-28.02$ (4)	$+0.48$
<b>4</b>	18.88	$-243.5$ (103)	$-59.79$ (24)	$-5.45$
<b>5</b>	2.99	$-159.5$ (25)	$-37.60$ (5)	$-2.04$
<b>6</b>	61.41	$-292.5$ (106)	$-72.95$ (25)	$-7.64$

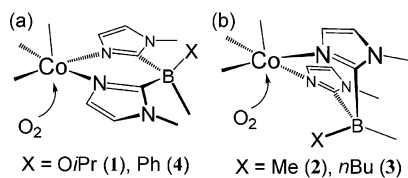
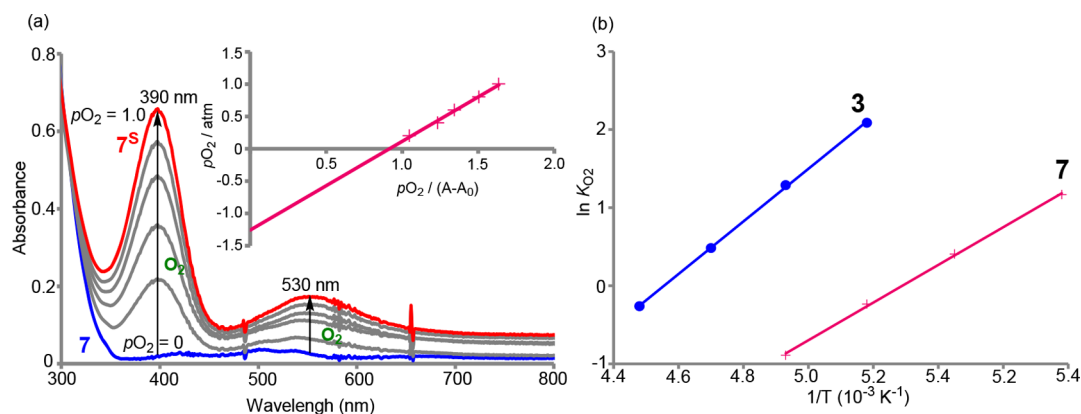


**Figure 5.** Schematic drawings of the structural difference of the cobalt centers depending on  $L^X$ .

different properties of  $X$  affected the strength of the  $\text{Co}-\text{O}_2^-$  bonds (i.e., the enthalpy change).

To clarify the effects of the steric and electronic properties of the bidentate ligands, the  $O_2$  affinity of Bp complex **7** was also investigated as a control. A solution of **7** was reacted with  $O_2$  at

low temperature to give the corresponding  $O_2$  adduct  $7^S$ , which showed two intense bands at approximately  $390$  nm ( $\epsilon = 1100\text{ M}^{-1}\text{cm}^{-1}$ ) and  $530$  nm ( $\epsilon = 300\text{ M}^{-1}\text{cm}^{-1}$ ) at  $-80\text{ }^\circ\text{C}$  (Figure S16), as observed for  $1^S$ – $4^S$ . A few related penta-coordinated cobalt(II) complexes with a combination of  $\text{Tp}^R$  and bis(pyrazolyl)borate ligands exist, but the  $O_2$  binding ability of these complexes has not yet been reported.<sup>65,66</sup> As described above, the shielding extent of the cobalt(II) center of **7** is close to those of **1** ( $X = \text{OiPr}$ ) and **4** ( $\text{Ph}$ ). Such structural property of **7** derived from the less-hindered Bp ligand would be an advantage to access  $O_2$  to the cobalt(II) center. Therefore, the  $O_2$  affinity of **7** was compared with those of **1–4**. The  $K_{O_2}$  value between **7** and  $7^S$  was  $0.79\text{ atm}^{-1}$  at  $-80\text{ }^\circ\text{C}$  and was smaller than the  $K_{O_2}$  value between **3** and  $3^S$  ( $8.07$ ),

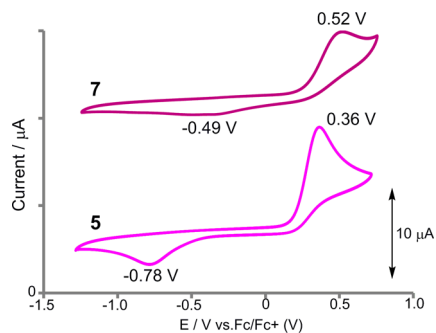


**Figure 6.** (a) Spectral changes of **7** under various  $O_2$  partial pressures ( $= p(O_2)$ ) in THF at  $-80\text{ }^\circ\text{C}$ .  $p(O_2) = 0, 0.2, 0.4, 0.6, 0.8,$  and  $1.0$  atm. The initial spectrum of **7** ( $p(O_2) = 0$  atm) is shown in the blue line, and the final saturated spectrum when  $p(O_2) = 1.0$  atm is the red line. The inset shows a plot of  $p(O_2)$  vs  $p(O_2)/(A - A_0)$  at  $390$  nm. (b) van't Hoff plots for the oxygenation of cobalt(II) complexes **3** and **7**.

Table 3. Equilibrium Constants and Thermodynamic Parameters of Co(II) Complexes 3 and 7 at  $-80^{\circ}\text{C}$ 

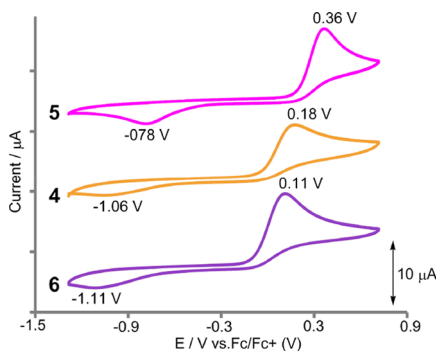
complex	$K_{\text{O}_2}$ at $-80^{\circ}\text{C}$ ( $\text{atm}^{-1}$ )	$\Delta S$ ( $\text{J}\cdot\text{K}^{-1}\cdot\text{mol}^{-1}$ )	$\Delta H$ ( $\text{kJ}\cdot\text{mol}^{-1}$ )	$\Delta G$ at $-80^{\circ}\text{C}$ ( $\text{kJ}\cdot\text{mol}^{-1}$ )
3	8.07	-127.6 (18)	-28.02 (4)	-3.35
7	0.79	-106.1 (22)	-20.06 (4)	+0.39

which was lowest in the series of  $L^X$  complexes 1–4 with the same  $\text{Tp}^{\text{Me}_2,4\text{H}}$  due to the shielding effect of  $n\text{Bu}$ , at the same temperature (Figure 6, Table 3). Moreover,  $\Delta H$  for the oxygenation of 7 was  $-20.1\text{ kJ mol}^{-1}$ , which was more positive (less favorable toward oxygenation) than that for 3 (see above). In Bp complex 7, the oxidation potential of cobalt(II) to cobalt(III) was  $0.52\text{ V}$  (Figure 7), which was higher than the

Figure 7. Cyclic voltammograms of 5 and 7 in  $\text{CH}_2\text{Cl}_2$  with  $0.1\text{ M } n\text{Bu}_4\text{NPF}_6$ .

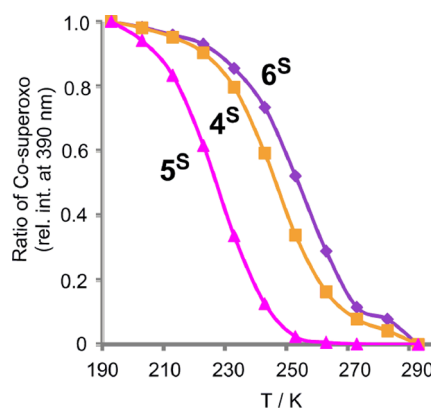
potentials observed for 1–4. These electrochemical trends are consistent with the lower Lewis basicity of pyrazole compared to that of 1-methylimidazole.<sup>68</sup> Therefore, these observations suggest that the electronic property of Bp rather than its structural property is responsible for the low  $\text{O}_2$  affinity of 7, whereas the  $\text{O}_2$  affinity of  $L^X$  complexes 1–4 is mainly controlled by the steric properties.

**2.2.2. Electronic Effects of  $\text{Tp}^{\text{Me}_2,4\text{R}}$ .** Then, we examined the effects of R on  $\text{Tp}^{\text{Me}_2,4\text{R}}$ . In the series of  $L^{\text{Ph}}$  complexes 4–6, the cobalt(II)/cobalt(III) oxidation potentials followed the order 6 (R = Me;  $0.11\text{ V}$ ) < 4 (H;  $0.18\text{ V}$ ) < 5 (Br;  $0.36\text{ V}$ ), as expected from the electronic properties of R (Figure 8). Both 5 and 6 reacted with  $\text{O}_2$  to give the corresponding cobalt(III)-superoxo species, as evidenced by the observation of two intense absorption bands in their UV–vis spectra (Figures S12 and S13). Notably, in complex  $5^{\text{S}}$  with the brominated ligand, these two bands were red-shifted compared to those in  $4^{\text{S}}$  and  $6^{\text{S}}$ . In complex  $5^{\text{S}}$ , the electron-withdrawing nature of the

Figure 8. Cyclic voltammograms of 4–6 in  $\text{CH}_2\text{Cl}_2$  with  $0.1\text{ M } n\text{Bu}_4\text{NPF}_6$ .

bromine substituent on  $\text{Tp}^{\text{Me}_2,4\text{Br}}$  weakened the ligand field, which lowered the energy levels of the empty  $d_{x^2-y^2}$  and  $d_{z^2}$  orbitals of the low-spin cobalt(III) center. In contrast, the  $\lambda_{\text{max}}$  values of the bands of  $6^{\text{S}}$  were similar to those of  $4^{\text{S}}$ . However, the molar absorption coefficients of the absorption bands followed the order  $5^{\text{S}} > 4^{\text{S}} > 6^{\text{S}}$ . Therefore, the overlap between the orbitals of cobalt and  $\text{O}_2^-$  increased with decreasing electron donation from  $\text{Tp}^{\text{Me}_2,4\text{R}}$ . The observed trends can be explained by the trans influence between the axial pyrazole donor and the superoxide ligand.

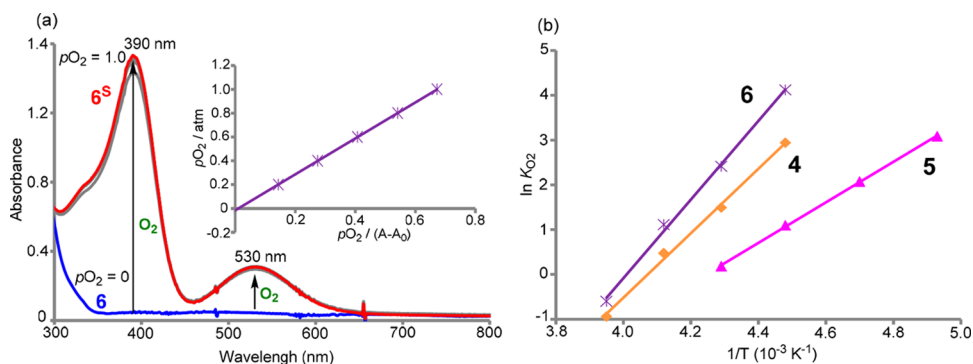
The order of thermal stability was  $6^{\text{S}} > 4^{\text{S}} > 5^{\text{S}}$ , which was estimated in a similar manner as that for  $1^{\text{S}}-4^{\text{S}}$  (Figure 9).

Figure 9. Thermal stability of  $4^{\text{S}}-6^{\text{S}}$  in  $0.16\text{ mM THF}$  solution.

Additionally, the  $K_{\text{O}_2}$  values determined at  $-50^{\circ}\text{C}$  were  $61.4\text{ atm}^{-1}$  for 6,  $18.9\text{ atm}^{-1}$  for 4, and  $3.0\text{ atm}^{-1}$  for 5. These trends were consistent with the order of the oxidation potentials of the cobalt(II) precursors. In addition, the  $\Delta H$  values (in  $\text{kJ mol}^{-1}$ ) for the oxygenation of each complex were  $-73.0$  (for 6),  $-59.8$  (4), and  $-37.6$  (5) (Figure 10). Therefore, the electronic properties of R directly affected the enthalpic stability of the cobalt(III)-superoxo species. Notably, the oxidation potentials of the cobalt(II) centers of  $\text{Tp}^{\text{Me}_2,4\text{H}}-L^{\text{alkyl}}$  complexes 2 ( $0.07\text{ V}$ ) and 3 ( $0.12\text{ V}$ ) were close to that of the complex with the highest  $\text{O}_2$  affinity (6;  $0.11\text{ V}$ ), which was composed of  $L^{\text{Ph}}$  and  $\text{Tp}^{\text{Me}_2,4\text{Me}}$ . The  $K_{\text{O}_2}$  value for 6 at  $-50^{\circ}\text{C}$  was 20–80 times larger than those for 2 and 3. These facts indicate that the steric effect from  $L^X$  is dominant to the  $\text{O}_2$  affinity of the cobalt(II) centers of which the oxidation potentials show close values.

### 3. CONCLUSION

We have revealed the effects of the distal substituent groups in the ligands on the  $\text{O}_2$  affinity of the supported metal center. The structural properties of the boron-attached group X on  $L^X$  affect the shielding percentage of the cobalt(II) centers and are critical for changing the enthalpic stabilization of the cobalt- $\text{O}_2$  adducts, although dependence of the electrochemical properties of the metal centers on X is inconsistent with the  $\text{O}_2$  affinities. Such unprecedented behavior arises from the structural flexibility of  $L^X$ . On the other hand, the electronic



**Figure 10.** (a) Spectral changes of **6** at various  $O_2$  partial pressures ( $= p(O_2)$ ) in THF at  $-50\text{ }^\circ\text{C}$ .  $p(O_2) = 0, 0.2, 0.4, 0.6, 0.8,$  and  $1.0$  atm starting from the bottom. The inset shows a plot of  $p(O_2)$  vs  $p(O_2)/(A - A_0)$  at  $390$  nm. (b) van't Hoff plots for the oxygenation of the cobalt(III)-superoxo complexes (**4**<sup>S</sup>–**6**<sup>S</sup>).

properties of the R substituent attached to the fourth position of the pyrazolyl rings of the rigid  $Tp^{Me_2,4R}$  ligands are reflected in the electrochemical nature and the  $O_2$  affinity of the metal center. In summary, the  $O_2$  affinity of the five azole-supported metal centers is controlled by the structural and electronic properties of the ligand substituent groups located in the secondary coordination sphere.

#### 4. EXPERIMENTAL

**4.1. General.** Elemental analysis was performed on a Perkin-Elmer CHNS/O analyzer 2400II. IR spectra were recorded on a JASCO FT/IR 4200 spectrometer with solid samples (as KBr pellets). NMR spectra were recorded on a JEOL ECA-600 spectrometer. UV–vis spectra were measured on an Agilent 8453 UV–vis spectrometer with a UNISOK CoolSpeK cell holder. Cyclic voltammetry was performed on an ALS Model 600C electrochemical analyzer. All commercial reagents and solvents were used without further purification unless otherwise noted. The preparation of oxygen-sensitive compounds was performed by Schlenk techniques under an Ar atmosphere.  $L^X$  ( $X = OiPr, Me, nBu, Ph$ )<sup>14,17</sup> and  $[Co^{II}(Tp^{Me_2,4R})(OAc)]$  ( $R = H, Me, Br$ )<sup>63</sup> were prepared according to the literature.

**4.2. X-ray Diffraction Study.** Diffraction data were collected for a single crystal of **2** using Rigaku “VariMax Mo” optics and multilayer mirror monochromated Mo- $K\alpha$  radiation with a Saturn70 CCD detector at the Institute for Materials Chemistry and Engineering, Kyushu University. Diffraction data for single crystals of **3**, **5**, **6**, and **7** were collected using a Rigaku Saturn 70 CDD area detector system with graphite monochromated Mo- $K\alpha$  radiation at Kanagawa University. The block- (**2**, **3**, **5**, **6**) or plate (**7**)-shaped crystals were mounted on a cryoloop with liquid paraffin and flash cooled to  $113$  K (for **3**, **5**, **6**),  $123$  K (for **2**), or  $193$  K (for **7**) by a flow of cold  $N_2$  gas on the goniometer. For complex **2**, two sets of data sweeps (at  $\phi = 90$  and  $270^\circ$ ) were conducted using  $\omega$  oscillations (sweep 1:  $\omega = -110.0$  to  $40.0^\circ$  at  $\phi = 90^\circ$  and sweep 2:  $\omega = -35.0$  to  $40.0^\circ$  at  $\phi = 270^\circ$ ) with  $0.5^\circ$  steps at  $\chi = 45^\circ$  with an exposure rate of  $4.0$  [s/ $^\circ$ ]. The detector swing angle was  $-20^\circ$ , and the crystal-to-detector distance was  $45$  mm (total of 450 oscillation images). For complex **3**, two sets of data sweeps (at  $\phi = 0$  and  $90^\circ$ ) were conducted using  $\omega$  oscillations from  $-110.0$  to  $70.0^\circ$  in  $0.5^\circ$  steps at  $\chi = 45^\circ$  with an exposure rate of  $36.0$  [s/ $^\circ$ ]. The detector swing angle was  $-20^\circ$ , and the crystal-to-detector distance was  $45$  mm (total of 720 oscillation images). For complexes **5**, **6**, and **7**, three sets of data sweeps (at  $\phi = 0, 90,$  and  $180^\circ$ ) were conducted using  $\omega$  oscillations from  $-115.0$  to  $65.0^\circ$  in  $0.3^\circ$  steps at  $\chi = 45^\circ$  with exposure rates of  $100.0$  [s/ $^\circ$ ] (for **5**),  $50.0$  [s/ $^\circ$ ] (for **6**), and  $133.3$  [s/ $^\circ$ ] (for **7**). The detector swing angle was  $-25^\circ$ , and the crystal-to-detector distance was  $55$  mm (total of 1800 oscillation images). Data collection and processing were performed using Rigaku CrystalClear software.<sup>69</sup> In total, 14717 reflections (**2**,  $R_{int} = 0.1030$ ), 11107 reflections (**3**,  $R_{int} = 0.0618$ ), 15476 reflections (**5**,  $R_{int} = 0.0260$ ), 14782 reflections (**6**,  $R_{int} =$

$0.0270$ ), and 11440 reflections (**7**,  $R_{int} = 0.0714$ ) were collected. The equivalent reflections were merged. The linear absorption coefficient,  $\mu$ , for Mo- $K\alpha$  radiation was  $6.01$   $cm^{-1}$  for **2**,  $5.93$   $cm^{-1}$  for **3**,  $40.31$   $cm^{-1}$  for **5**,  $5.31$   $cm^{-1}$  for **6**, and  $7.10$   $cm^{-1}$  for **7**. A numerical absorption correction was applied and resulted in transmission factors ranging from  $0.8893$  to  $0.8893$  for **2**, from  $0.8813$  to  $0.9103$  for **3**, from  $0.5193$  to  $0.5843$  for **5**, from  $0.8646$  to  $0.9366$  for **6**, and from  $0.8528$  to  $0.9586$  for **7**. The data were corrected for Lorentz and polarization effects. Structural solution by a direct method (SIR-92)<sup>70</sup> and refinement by full-matrix least-squares (SHELXL-2014/7)<sup>71</sup> against  $F^2$  with all reflections were performed on WinGX software.<sup>72</sup> All nonhydrogen atoms were refined anisotropically. Hydrogen atoms adjacent to carbon atoms were placed in calculated positions with C–H =  $0.96$  Å (for methyl groups) or  $0.93$  Å (for aromatic rings) with Uiso(H) =  $1.2$  Uiso(attached atom). Hydrogen atoms on boron atoms were located by difference Fourier synthesis and refined isotropically with B–H =  $1.10$  Å. The molecular structure was drawn in the ORTEP-3 for Windows program.<sup>73</sup> Crystal information files (CIF) of the complexes reported in this paper have been deposited with the Cambridge Crystallographic Data Centre as supplementary publications CCDC-1843685 (**2**) CCDC-1843686 (**3**), CCDC-1843687 (**5**), CCDC-1843688 (**6**), and CCDC-1893689 (**7**). These data can be obtained free of charge from the Cambridge Crystallographic Data Centre at [www.ccdc.cam.ac.uk/data\\_request/cif](http://www.ccdc.cam.ac.uk/data_request/cif). The crystallographic data and structure refinement parameters of the three catalysts are given in Table S1.

**4.3. Preparation and Characterization Cobalt(II) Complexes.** **4.3.1.  $[Co^{II}(Tp^{Me_2,4R})(L^X)]$  (**1**–**6**).** As a typical example, the synthetic procedure is described for cobalt(II) complex **1**. A THF suspension ( $30$  mL) of  $LiL^{OiPr}$  ( $241.2$  mg,  $0.949$  mmol) was slowly added into a THF solution ( $30$  mL) of  $[Co^{II}(Tp^{Me_2,4H})(OAc)]$  ( $440$  mg,  $1.06$  mmol). After stirring for  $4$  h, the volatile solvent was evaporated, and the residue was redissolved in  $CH_2Cl_2$ . The solution was then passed through a filter with Celite to remove any inorganic salts. After evaporation of  $CH_2Cl_2$ , the residue was redissolved in MeCN, and the solution was passed through a filter with Celite. After reduction of the solvent volume by evaporation, the solution was subjected to recrystallization at  $-30\text{ }^\circ\text{C}$  to give the title complex as a red-purple powder ( $178$  mg,  $0.295$  mmol,  $31.1\%$ ). Recrystallization from a  $CH_2Cl_2$ /MeCN solution at  $-30\text{ }^\circ\text{C}$  gave a red needle crystal suitable for X-ray crystallography.

$[Co^{II}(Tp^{Me_2,4H})(L^{OiPr})]$  (**1**). FT/IR (KBr):  $\nu = 3124$  (w),  $2980$  (m),  $2961$  (vs),  $2927$  (vs),  $2865$  (vs),  $2512$  (m,  $\nu_{BH}$ ),  $1283$   $cm^{-1}$  (vs,  $\nu_{BC}$ ). UV–vis ( $CH_2Cl_2$ , r.t.):  $\lambda = 532$  nm ( $\epsilon = 94.2$   $M^{-1}$   $cm^{-1}$ ),  $505$  nm ( $\epsilon = 94.2$   $M^{-1}$   $cm^{-1}$ ),  $427$  nm ( $\epsilon = 72.1$   $M^{-1}$   $cm^{-1}$ ).  $^1H$  NMR ( $600$  MHz,  $CDCl_3$ ,  $25\text{ }^\circ\text{C}$ , TMS):  $\delta = 54.97$  (br, 1H;  $iPr$ ),  $42.41$  (br, 3H; Pz-H),  $38.41$  (br, 9H; Pz- $CH_3$ ),  $37.35$  (br, 6H; Im- $CH_3$ ),  $30.83$  (br, 2H; Im),  $25.31$  (br, 3H; B- $CH_3$ ),  $23.53$  (br, 6H;  $iPr$ ),  $-55.45$  (br, 2H; Pz- $CH_3$ ),  $-71.31$  (br, 6H; Pz- $CH_3$ ). ESI-MS<sup>+</sup> (MeCN):  $m/z = 603$  ( $M^+$ ). Magnetic moment (Evans method, r.t.,  $CDCl_3$ ):  $\mu_{eff} = 4.1$   $\mu_B$ . Elemental analysis calcd (%) for  $[Co^{II}(Tp^{Me_2,4H})(L^{OiPr})]$



(C<sub>27</sub>H<sub>42</sub>N<sub>10</sub>B<sub>2</sub>OCo): C 53.76, H 7.02, N 23.22; found: C 53.39, H 6.75, N 22.98.

The other complexes were prepared by following the same procedure. In the synthesis of the complexes 2–6, LiL<sup>X</sup>, which was generated by the reaction of HL<sup>X</sup> with *n*-butyllithium at –80 °C, reacted with the corresponding acetate complexes [Co<sup>II</sup>(Tp<sup>Me2,4R</sup>)(OAc)] (where R = H for 2–4, Br for 5, and Me for 6, respectively).

[Co<sup>II</sup>(Tp<sup>Me2,4H</sup>)(L<sup>Me</sup>)] (2). The crude complex was recrystallized from MeCN at –30 °C to give the title complex as a light pink powder (50.7 mg, 0.091 mmol, 46.4%). Recrystallization from a CH<sub>2</sub>Cl<sub>2</sub>/MeCN solution at –30 °C gave a red block crystal suitable for X-ray crystallography. FT-IR (KBr):  $\nu = 3117$  (w), 2911 (vs), 2517 (m,  $\nu_{\text{BH}}$ ), 1287 cm<sup>-1</sup> (vs,  $\nu_{\text{BC}}$ ). UV–vis (CH<sub>2</sub>Cl<sub>2</sub>, r.t.):  $\lambda = 537$  nm ( $\epsilon = 60.0$  M<sup>-1</sup> cm<sup>-1</sup>), 500 nm ( $\epsilon = 71.8$  M<sup>-1</sup> cm<sup>-1</sup>), 420 nm ( $\epsilon = 71.0$  M<sup>-1</sup> cm<sup>-1</sup>). <sup>1</sup>H NMR (600 MHz, CDCl<sub>3</sub>, 25 °C, TMS):  $\delta = 59.01$  (s, 1H; B-H), 37.98 (s, 3H; Pz-H), 31.14 (s, 2H; Im), 29.60 (s, 6H; Im-CH<sub>3</sub>), 25.96 (br, 9H; Pz-CH<sub>3</sub>), 1.54 (s, 6H; B-CH<sub>3</sub>), –17.77 (br, 2H; Im), –43.88 (br, 9H; Pz-CH<sub>3</sub>). ESI-MS<sup>+</sup> (MeCN):  $m/z = 388$  ([M – L<sup>Me</sup> + MeCN]<sup>+</sup>), 544 ([M – CH<sub>3</sub>]<sup>+</sup>). Magnetic moment (Evans method, r.t., CDCl<sub>3</sub>):  $\mu_{\text{eff}} = 3.5$   $\mu_{\text{B}}$ . Elemental analysis calcd (%) for [Co<sup>II</sup>(Tp<sup>Me2,4H</sup>)(L<sup>Me</sup>)] (C<sub>25</sub>H<sub>38</sub>N<sub>10</sub>B<sub>2</sub>Co): C 53.70, H 6.85, N 25.05; found: C 53.65, H 7.06, N 24.79.

[Co<sup>II</sup>(Tp<sup>Me2,4H</sup>)(L<sup>nBu</sup>)] (3). The crude complex was recrystallized from MeCN at –30 °C to give the title complex as a brown powder (89.5 mg, 0.149 mmol, 30.3%). Further recrystallization from a CH<sub>2</sub>Cl<sub>2</sub>/MeCN solution at –30 °C gave a brown block crystal suitable for X-ray crystallography. FT-IR (KBr):  $\nu = 3120$  (w), 2948 (vs), 2925 (vs), 2866 (vs), 2511 (m,  $\nu_{\text{BH}}$ ), 1285 cm<sup>-1</sup> (m,  $\nu_{\text{BC}}$ ). UV–vis (CH<sub>2</sub>Cl<sub>2</sub>, r.t.):  $\lambda = 539$  nm ( $\epsilon = 77.8$  M<sup>-1</sup> cm<sup>-1</sup>), 501 nm ( $\epsilon = 89.2$  M<sup>-1</sup> cm<sup>-1</sup>), 420 nm ( $\epsilon = 79.4$  M<sup>-1</sup> cm<sup>-1</sup>). <sup>1</sup>H NMR (600 MHz, CDCl<sub>3</sub>, 25 °C, TMS):  $\delta = 58.83$  (br, 1H; B-H), 36.78 (s, 3H; Pz-CH<sub>3</sub>), 30.41 (br, 2H; Im), 29.49 (br, 2H; <sup>n</sup>Bu-CH<sub>2</sub>), 28.33 (s, 6H; Im-CH<sub>3</sub>), 25.54 (br, 9H; Pz-CH<sub>3</sub>), 1.49 (br, 3H; B-CH<sub>3</sub>), –10.32 (s, 3H; <sup>n</sup>Bu-CH<sub>3</sub>), –16.14 (br, 2H; Im), –21.91 (s, 2H; <sup>n</sup>Bu-CH<sub>2</sub>), –22.80 (br, 2H; <sup>n</sup>Bu-CH<sub>2</sub>), –44.15 (s, 9H; Pz-CH<sub>3</sub>). ESI-MS<sup>+</sup> (MeCN):  $m/z = 544$  ([M – C<sub>4</sub>H<sub>9</sub>]<sup>+</sup>). Magnetic moment (Evans method, r.t., CDCl<sub>3</sub>):  $\mu_{\text{eff}} = 3.6$   $\mu_{\text{B}}$ . Elemental analysis calcd (%) for [Co<sup>II</sup>(Tp<sup>Me2,4H</sup>)(L<sup>nBu</sup>)] (C<sub>28</sub>H<sub>44</sub>N<sub>10</sub>B<sub>2</sub>Co): C 55.93, H 7.38, N 23.30; found: C 55.68, H 7.01, N 23.25.

[Co<sup>II</sup>(Tp<sup>Me2,4H</sup>)(L<sup>Ph</sup>)] (4). The crude complex was recrystallized from DMF at –30 °C to give the title complex as a brown powder (45.1 mg, 0.073 mmol, 7.4%). Recrystallization from a CH<sub>2</sub>Cl<sub>2</sub>/MeCN solution at –30 °C gave a red block crystal suitable for X-ray crystallography. FT-IR (KBr):  $\nu = 3120$  (w), 2953 (vs), 2909 (vs), 2513 (m,  $\nu_{\text{BH}}$ ), 1285 cm<sup>-1</sup> (m,  $\nu_{\text{BC}}$ ). UV–vis (CH<sub>2</sub>Cl<sub>2</sub>, r.t.):  $\lambda = 663$  nm ( $\epsilon = 21.1$  M<sup>-1</sup> cm<sup>-1</sup>), 496 nm ( $\epsilon = 91.2$  M<sup>-1</sup> cm<sup>-1</sup>). <sup>1</sup>H NMR (600 MHz, CDCl<sub>3</sub>, 25 °C, TMS):  $\delta = 48.87$  (br, 1H; B-H), 32.51 (br, 3H; Pz-H), 30.37 (br, 2H; Im), 20.46 (br, 9H; Pz-CH<sub>3</sub>), 19.94 (br, 6H; Im-CH<sub>3</sub>), 15.25 (br, 2H; Ph), 13.56 (br, 2H; Ph), 13.49 (br, 1H; Ph), 4.19 (br, 3H; B-CH<sub>3</sub>), –18.93 (br, 2H; Im), –37.67 (br, 9H; Pz-CH<sub>3</sub>). ESI-MS<sup>+</sup> (MeCN):  $m/z = 606$  ([M – CH<sub>3</sub>]<sup>+</sup>), 397 ([M – L<sup>Ph</sup> + MeCN]<sup>+</sup>). Magnetic moment (Evans method, r.t., CDCl<sub>3</sub>):  $\mu_{\text{eff}} = 3.6$   $\mu_{\text{B}}$ . Elemental analysis calcd (%) for [Co<sup>II</sup>(Tp<sup>Me2,4H</sup>)(L<sup>Ph</sup>)] (C<sub>36</sub>H<sub>40</sub>N<sub>10</sub>B<sub>2</sub>Co): C 58.00, H 6.49, N 22.55; found: C 57.60, H 6.29, N 22.38.

[Co<sup>II</sup>(Tp<sup>Me2,4Br</sup>)(L<sup>Ph</sup>)] (5). The crude complex was washed with a small amount of pentane to give the title complex as a beige powder (130 mg, 0.152 mmol, 22.7%). Recrystallization from a CH<sub>2</sub>Cl<sub>2</sub>/*i*PrOH solution at room temperature gave a pale brown block crystal suitable for X-ray crystallography. FT-IR (KBr):  $\nu = 3125$  (w), 3045 (w), 2989 (w), 2955 (w), 2902 (vs), 2521 (s,  $\nu_{\text{BH}}$ ), 1285 cm<sup>-1</sup> (s,  $\nu_{\text{BC}}$ ). UV–vis (CH<sub>2</sub>Cl<sub>2</sub>, r.t.):  $\lambda = 684$  nm ( $\epsilon = 21.6$  M<sup>-1</sup> cm<sup>-1</sup>), 493 nm ( $\epsilon = 98.2$  M<sup>-1</sup> cm<sup>-1</sup>). <sup>1</sup>H NMR (600 MHz, CDCl<sub>3</sub>, 25 °C, TMS):  $\delta = 46.68$  (br, 1H; B-H), 29.72 (s, 2H; Im), 19.46 (br, 9H; Pz-CH<sub>3</sub>), 19.02 (s, 6H; Im-CH<sub>3</sub>), 15.04 (s, 2H; Ph), 13.33 (s, 1H; Ph), 12.74 (s, 2H; Ph), 2.37 (br, 3H; B-CH<sub>3</sub>), –16.22 (br, 2H; Im), –36.38 (br, 9H; Pz-CH<sub>3</sub>). ESI-MS<sup>+</sup> (MeCN):  $m/z = 899$  ([M + MeCN + H]<sup>+</sup>). Magnetic moment (Evans method, r.t., CDCl<sub>3</sub>):  $\mu_{\text{eff}} = 3.3$   $\mu_{\text{B}}$ . Elemental analysis calcd (%) for [Co<sup>II</sup>(Tp<sup>Me2,4Br</sup>)(L<sup>Ph</sup>)]

(C<sub>30</sub>H<sub>37</sub>N<sub>10</sub>B<sub>2</sub>Br<sub>3</sub>Co): C 42.00, H 4.35, N 16.33; found: C 41.70, H 4.53, N 15.94.

[Co<sup>II</sup>(Tp<sup>Me2,4Me</sup>)(L<sup>Ph</sup>)] (6). The crude complex was recrystallized from MeCN at –30 °C to give the title complex as a reddish-brown powder (173 mg, 0.261 mmol, 11.7%). Recrystallization from a MeCN solution at –30 °C gave a red block crystal suitable for X-ray crystallography. FT-IR (KBr):  $\nu = 3119$  (w), 3041 (w), 2995 (w), 2913 (vs), 2860 (m), 2505 (vs,  $\nu_{\text{BH}}$ ), 1284 cm<sup>-1</sup> (s,  $\nu_{\text{BC}}$ ). UV–vis (CH<sub>2</sub>Cl<sub>2</sub>, r.t.):  $\lambda = 681$  nm ( $\epsilon = 27.7$  M<sup>-1</sup> cm<sup>-1</sup>), 498 nm ( $\epsilon = 116.7$  M<sup>-1</sup> cm<sup>-1</sup>), 420 nm ( $\epsilon = 103.3$  M<sup>-1</sup> cm<sup>-1</sup>). <sup>1</sup>H NMR (600 MHz, CDCl<sub>3</sub>, 25 °C, TMS):  $\delta = 56.81$  (br, 1H; B-H), 33.61 (br, 2H; Im), 23.67 (s, 9H; Pz-CH<sub>3</sub>), 22.43 (s, 6H; Im-CH<sub>3</sub>), 16.36 (s, 2H; Ph), 15.81 (s, 2H; Ph), 14.34 (s, 1H; Ph), 7.28 (br, 9H; Pz-CH<sub>3</sub>), 6.10 (s, 3H; B-CH<sub>3</sub>), –24.90 (br, 2H; Im), –43.24 (br, 9H; Pz-CH<sub>3</sub>). ESI-MS<sup>+</sup> (MeCN):  $m/z = 664$  ([M + H]<sup>+</sup>). Magnetic moment (Evans method, r.t., CDCl<sub>3</sub>):  $\mu_{\text{eff}} = 3.4$   $\mu_{\text{B}}$ . Elemental analysis calcd (%) for [Co<sup>II</sup>(Tp<sup>Me2,4Me</sup>)(L<sup>Ph</sup>)]·0.5H<sub>2</sub>O (C<sub>33</sub>H<sub>47</sub>N<sub>10</sub>B<sub>2</sub>CoO<sub>0.5</sub>): C 58.95, H 7.05, N 20.83; found: C 58.89, H 7.25, N 20.94.

4.3.2. [Co<sup>II</sup>(Tp<sup>Me2,4H</sup>)(Bp)] (7). This Bp complex was also synthesized by the same procedure for 1, where KBp was used instead of LiL<sup>OPr</sup>. This complex was recrystallized from MeCN at –30 °C to give the title complex as a red-purple powder (193.3 mg, 0.348 mmol, 38.9%). Recrystallization from a CH<sub>2</sub>Cl<sub>2</sub>/pentane solution at room temperature gave a red block crystal suitable for X-ray crystallography. FT-IR (KBr):  $\nu = 3133$  (w), 2959 (vs), 2927 (vs), 2861 (vs), 2509 (vs,  $\nu_{\text{BH}}$ ), 2432 cm<sup>-1</sup> (vs,  $\nu_{\text{BH}}$ ). UV–vis (CH<sub>2</sub>Cl<sub>2</sub>, r.t.):  $\lambda = 537$  nm ( $\epsilon = 77.4$  M<sup>-1</sup> cm<sup>-1</sup>), 506 nm ( $\epsilon = 81.5$  M<sup>-1</sup> cm<sup>-1</sup>), 422 nm ( $\epsilon = 55.0$  M<sup>-1</sup> cm<sup>-1</sup>). <sup>1</sup>H NMR (600 MHz, CDCl<sub>3</sub>, 25 °C, TMS):  $\delta = 137.04$  (br, 2H; B(Bp)-H), 74.54 (br, 1H; Pz(Tp)-H), 73.15 (s, 2H; Pz(Tp)-H), 55.76 (s, 2H; Pz(Bp)-H), 45.95 (s, 3H; Pz(Tp)-CH<sub>3</sub>), 44.88 (s, 6H; Pz(Tp)-CH<sub>3</sub>), 16.16 (s, 2H; Pz(Bp)-H), –49.48 (s, 6H; Pz(Tp)-CH<sub>3</sub>), –50.68 (s, 3H; Pz(Tp)-CH<sub>3</sub>), –67.03 (s, 2H; Pz(Bp)-H). ESI-MS<sup>+</sup> (MeOH):  $m/z = 503$  (M<sup>+</sup>). Magnetic moment (Evans method, r.t., CDCl<sub>3</sub>):  $\mu_{\text{eff}} = 4.2$   $\mu_{\text{B}}$ . Elemental analysis calcd (%) for [Co<sup>II</sup>(Tp<sup>Me2,4H</sup>)(Bp)] (C<sub>21</sub>H<sub>30</sub>N<sub>10</sub>B<sub>2</sub>Co): C 50.14, H 6.01, N 27.84; found: C 49.70, H 5.53, N 27.39.

#### 4.4. Thermodynamic Analysis of the Oxygenation of 1–7.

UV–vis spectra of 1–7 in THF were measured at low temperature under various O<sub>2</sub> partial pressures ( $p(\text{O}_2)$ ). Argon and dioxygen gas were mixed using two mass flow controllers and passed through approximately 0.17 mM solutions (gas flow 100 mL min<sup>-1</sup>) of the complex in a quartz cell (1 cm path length). The gas mixture was bubbled through the solution for 0.5 h before the measurement to ensure that equilibrium had been reached. The growth of absorption band shoulders, absent in the deoxy form, upon oxygenation were monitored at 390 nm. The strong binding affinity resulted in saturation at high  $p\text{O}_2$  values, and the measurements obtained at these partial pressures could not be used in the determination of the equilibrium constant ( $K_{\text{O}_2}$ ).

## ■ ASSOCIATED CONTENT

### Supporting Information

The Supporting Information is available free of charge on the ACS Publications website at DOI: 10.1021/acs.inorgchem.8b02241.

<sup>1</sup>H NMR spectra of the cobalt(II) complexes 1–7, drawings of the sphere-shielding of 1–7 and 1<sup>S</sup>, space filling diagrams of 1–7 and 1<sup>S</sup>, DR-UV–vis spectra of the solid samples of 6 and 6<sup>S</sup>, UV–vis spectra in the reversible O<sub>2</sub> sorption/desorption experiments on 1 and 3–7, IR spectra of *in situ* generated 2<sup>S</sup>–7<sup>S</sup> and 2–7 in CH<sub>2</sub>Cl<sub>2</sub> solutions, crystallographic data and structure refinement parameters for 1–7 and 1<sup>S</sup>, and  $K_{\text{O}_2}$  values of 1–7 under various temperatures (PDF)

## Accession Codes

CCDC 1843685–1843689 contain the supplementary crystallographic data for this paper. These data can be obtained free of charge via [www.ccdc.cam.ac.uk/data\\_request/cif](http://www.ccdc.cam.ac.uk/data_request/cif), or by emailing [data\\_request@ccdc.cam.ac.uk](mailto:data_request@ccdc.cam.ac.uk), or by contacting The Cambridge Crystallographic Data Centre, 12 Union Road, Cambridge CB2 1EZ, UK; fax: +44 1223 336033.

## AUTHOR INFORMATION

## Corresponding Authors

\*E-mail: [jnaka@kanagawa-u.ac.jp](mailto:jnaka@kanagawa-u.ac.jp).

\*E-mail: [hikichi@kanagawa-u.ac.jp](mailto:hikichi@kanagawa-u.ac.jp).

## ORCID

Jun Nakazawa: 0000-0003-4665-6657

Shiro Hikichi: 0000-0001-6001-9780

## Notes

The authors declare no competing financial interest.

## ACKNOWLEDGMENTS

This research was funded by CREST, JST (JPMJCR16P1), and Kanagawa University (ordinary budget for 411)

## REFERENCES

- (1) Ray, K.; Pfaff, F. F.; Wang, B.; Nam, W. Status of Reactive Non-Heme Metal–Oxygen Intermediates in Chemical and Enzymatic Reactions. *J. Am. Chem. Soc.* **2014**, *136*, 13942–13958.
- (2) Sahu, S.; Goldberg, D. P. Activation of Dioxygen by Iron and Manganese Complexes: A Heme and Nonheme Perspective. *J. Am. Chem. Soc.* **2016**, *138*, 11410–11428.
- (3) Elwell, C. E.; Gagnon, N. L.; Neisen, B. D.; Dhar, D.; Spaeth, A. D.; Yee, G. M.; Tolman, W. B. Copper–Oxygen Complexes Revisited: Structures, Spectroscopy, and Reactivity. *Chem. Rev.* **2017**, *117*, 2059–2107.
- (4) Solomon, E. I.; Stahl, S. S. Thematic Issue, “Oxygen Reduction and Activation in Catalysis”. *Chem. Rev.* **2018**, *118* (5), 2299–2862.
- (5) Riess, J. G. Oxygen Carriers (“Blood Substitutes”)—Raison d’Etre, Chemistry, and Some Physiology. *Chem. Rev.* **2001**, *101*, 2797–2919.
- (6) Li, G. Q.; Govind, R. Separation of Oxygen from Air Using Coordination Complexes: A Review. *Ind. Eng. Chem. Res.* **1994**, *33*, 755–783.
- (7) Yang, J.; Kloek, A. P.; Goldberg, D. E.; Mathews, F. S. The structure of Ascaris hemoglobin domain I at 2.2 Å resolution: Molecular features of oxygen avidity. *Proc. Natl. Acad. Sci. U. S. A.* **1995**, *92*, 4224–4228.
- (8) Holmes, M. A.; Le Trong, I.; Turley, S.; Sieker, L. C.; Stenkamp, R. E. Structures of deoxy and oxy hemerythrin at 2.0 Å resolution. *J. Mol. Biol.* **1991**, *218*, 583–593.
- (9) Magnus, K. A.; Hazes, B.; Ton-That, H.; Bonaventura, C.; Bonaventura, J.; Hol, W. G. J. Crystallographic analysis of oxygenated and deoxygenated states of arthropod hemocyanin shows unusual differences. *Proteins: Struct., Funct., Genet.* **1994**, *19*, 302–309.
- (10) Oddon, F.; Chiba, Y.; Nakazawa, J.; Ohta, T.; Ogura, T.; Hikichi, S. Characterization of Mononuclear Non-heme Iron(III)-Superoxo Complex with a Five-Azole Ligand Set. *Angew. Chem., Int. Ed.* **2015**, *54*, 7336–7339.
- (11) Trofimenko, S. *Scorpionates – The Coordination Chemistry of Polypyrazolylborate Ligands*; Imperial College Press: London, England, 1999.
- (12) Pettinari, C. *Scorpionates II: Chelating Borate Ligands*; Imperial College Press: London, England, 2008.
- (13) Fujita, K.; Hikichi, S.; Akita, M.; Moro-oka, Y. Novel monoanionic tripodal ligands: methylbis(1-methylimidazol-2-yl)-(pyrazol-1-yl)borate (= [MeB(Im<sup>N-Me</sup>)<sub>2</sub>(Pz<sup>R</sup>)]<sup>-</sup>). Synthesis and structural characterization of their nickel complexes and carboxylate shift from nickel to boron. *J. Chem. Soc., Dalton Trans.* **2000**, 117–120.
- (14) Fujita, K.; Hikichi, S.; Akita, M.; Moro-oka, Y. Synthesis and structural characterization of a new-class of organoborate ligands containing imidazolyl functional groups [MeB(Im<sup>N-Me</sup>)<sub>2</sub>(X)]<sup>-</sup>. *J. Chem. Soc., Dalton Trans.* **2000**, 1255–1260.
- (15) Hikichi, S.; Kaneko, M.; Miyoshi, Y.; Mizuno, N.; Fujita, K.; Akita, M. Design, Synthesis, and Catalysis of Bio-inspired Immobilized Metallocomplex Catalyst. *Top. Catal.* **2009**, *52*, 845–851.
- (16) Fujita, K.; Akita, M.; Hikichi, S. Acetoxybis(imidazolyl)-methylborate [B(Im<sup>N-Me</sup>)<sub>2</sub>(OC(=O)Me)Me]<sup>-</sup>: Carboxylation of borane moiety of imidazolyl-based scorpionate. *Inorg. Chim. Acta* **2009**, *362*, 4472–4479.
- (17) Hikichi, S.; Fujita, K.; Manabe, Y.; Akita, M.; Nakazawa, J.; Komatsuzaki, H. Coordination property of organoborate ligands: Steric hindrance around distal boron center direct the conformation of dialkylbis(imidazolyl)borate scaffold. *Eur. J. Inorg. Chem.* **2010**, *2010*, 5529–5537.
- (18) Tsuruta, T.; Yamazaki, T.; Watanabe, K.; Chiba, Y.; Yoshida, A.; Naito, S.; Nakazawa, J.; Hikichi, S. Mimicking the Active Sites of Non-heme Iron Oxygenases on the Solid Supports of Catalysts: Formation of Immobilized Iron Complexes with Imidazolyl and Carboxylate Ligands. *Chem. Lett.* **2015**, *44*, 144–146.
- (19) Ando, K.; Nakazawa, J.; Hikichi, S. Synthesis, Characterization and Aerobic Alcohol Oxidation Catalysis of Palladium(II) Complexes with a Bis(imidazolyl)borate Ligand. *Eur. J. Inorg. Chem.* **2016**, *2016*, 2603–2608.
- (20) Nishiura, T.; Uramoto, T.; Takiyama, Y.; Nakazawa, J.; Hikichi, S. Cobalt(II) Complexes with N,N,N-Scorpionates and Bidentate Ligands: Comparison of Hydrotris(3,5-dimethylpyrazol-1-yl)borate Tp\* vs. Phenyltris(4,4-dimethyloxazolin-2-yl)borate To<sup>M</sup> to Control the Structural Properties and Reactivities of Cobalt Centers. *Molecules* **2018**, *23*, 1466.
- (21) Hikichi, S.; Kobayashi, C.; Yoshizawa, M.; Akita, M. Tuning the Stability and Reactivity of Metal-bound Alkylperoxide by Remote Site Substitution of the Ligand. *Chem. - Asian J.* **2010**, *5*, 2086–2092.
- (22) Jones, R. D.; Summerville, D. A.; Basolo, F. Synthetic oxygen carriers related to biological systems. *Chem. Rev.* **1979**, *79*, 139–179.
- (23) Niederhoffer, E. C.; Timmons, J. H.; Martell, A. E. Thermodynamics of oxygen binding in natural and synthetic dioxygen complexes. *Chem. Rev.* **1984**, *84*, 137–203.
- (24) Busch, D. H.; Alcock, N. W. Iron and Cobalt “Lacunar” Complexes as Dioxygen Carriers. *Chem. Rev.* **1994**, *94*, 585–623.
- (25) Bianchini, C.; Zoellner, R. W. Activation of Dioxygen by Cobalt Group Metal Complexes. *Adv. Inorg. Chem.* **1996**, *44*, 263–339.
- (26) Hikichi, S.; Akita, M.; Moro-oka, Y. New Aspects of the Cobalt-Dioxygen Complex Chemistry Opened by Hydrotris(pyrazolyl)borate Ligands (Tp<sup>R</sup>): Unique Properties of Tp<sup>R</sup>Co-Dioxygen Complexes. *Coord. Chem. Rev.* **2000**, *198*, 61–87.
- (27) Fiedler, A. T.; Fischer, A. A. Oxygen activation by mononuclear Mn, Co, and Ni centers in biology and synthetic complexes. *JBIC, J. Biol. Inorg. Chem.* **2017**, *22*, 407–424.
- (28) Hoffman, B. M.; Petering, D. H. Coboglobins: Oxygen-Carrying Cobalt-Reconstituted Hemoglobin and Myoglobin. *Proc. Natl. Acad. Sci. U. S. A.* **1970**, *67*, 637–643.
- (29) Matsuo, T.; Tsuruta, T.; Maehara, K.; Sato, H.; Hisaeda, Y.; Hayashi, T. Preparation and O<sub>2</sub> binding study of myoglobin having a cobalt porphycene. *Inorg. Chem.* **2005**, *44*, 9391–9396.
- (30) Collman, J. P.; Yan, Y.-L.; Eberspacher, T.; Xie, X.; Solomon, E. I. Oxygen Binding of Water-Soluble Cobalt Porphyrins in Aqueous Solution. *Inorg. Chem.* **2005**, *44*, 9628–9630.
- (31) Ramdhanie, B.; Telsler, J.; Caneschi, A.; Zakharov, L. N.; Rheingold, A. L.; Goldberg, D. P. An Example of O<sub>2</sub> Binding in a Cobalt(II) Corrole System and High-Valent Cobalt-Cyano and Cobalt-Alkynyl Complexes. *J. Am. Chem. Soc.* **2004**, *126*, 2515–2525.
- (32) Rajani, C.; Kincaid, J. R.; Petering, D. H. Resonance Raman Studies of HOO-Co(III)Bleomycin and Co(III)Bleomycin: Identifi-

fication of Two Important Vibrational Modes,  $\nu(\text{Co-OOH})$  and  $\nu(\text{O-OH})$ . *J. Am. Chem. Soc.* **2004**, *126*, 3829–3836.

(33) Goodwin, K. D.; Lewis, M. A.; Long, E. C.; Georgiadis, M. M. Crystal structure of DNA-bound Co(III)-bleomycin B<sub>2</sub>: Insights on intercalation and minor groove binding. *Proc. Natl. Acad. Sci. U. S. A.* **2008**, *105*, S052–S056.

(34) Fielding, A. J.; Lipscomb, J. D.; Que, L., Jr. Characterization of an O<sub>2</sub> Adduct of an Active Cobalt-Substituted Extradiol-Cleaving Catechol Dioxygenase. *J. Am. Chem. Soc.* **2012**, *134*, 796–799.

(35) Cho, J.; Sarangi, R.; Kang, H. Y.; Lee, J. Y.; Kubo, M.; Ogura, T.; Solomon, E. I.; Nam, W. Synthesis, Structural, and Spectroscopic Characterization and Reactivities of Mononuclear Cobalt(III)-Peroxo Complexes. *J. Am. Chem. Soc.* **2010**, *132*, 16977–16986.

(36) Kim, D.; Cho, J.; Lee, Y.-M.; Sarangi, R.; Nam, W. Synthesis, Characterization, and Reactivity of Cobalt(III)-Oxygen Complexes Bearing a Macrocyclic N-Tetramethylated Cyclam Ligand. *Chem. - Eur. J.* **2013**, *19*, 14112–14118.

(37) Tcho, W.-Y.; Wang, B.; Lee, Y.-M.; Cho, K.-B.; Shearer, J.; Nam, W. A mononuclear nonheme cobalt(III)-hydroperoxide complex with an amphoteric reactivity in electrophilic and nucleophilic oxidative reactions. *Dalton Trans* **2016**, *45*, 14511–14515.

(38) Noh, H.; Jeong, D.; Ohta, T.; Ogura, T.; Valentine, J. S.; Cho, J. Distinct reactivity of a mononuclear peroxocobalt(III) species toward activation of nitriles. *J. Am. Chem. Soc.* **2017**, *139*, 10960–10963.

(39) Shin, B.; Sutherlin, K. D.; Ohta, T.; Ogura, T.; Solomon, E. I.; Cho, J. Reactivity of a Cobalt(III)-Hydroperoxo Complex in Electrophilic Reactions. *Inorg. Chem.* **2016**, *55*, 12391–12399.

(40) Wang, C.-C.; Chang, H.-C.; Lai, Y.-C.; Fang, H.; Li, C.-C.; Hsu, H.-K.; Li, Z.-Y.; Lin, T.-S.; Kuo, T.-S.; Neese, F.; Ye, S.; Chiang, Y.-W.; Tsai, M.-L.; Liaw, W.-F.; Lee, W.-Z. A Structurally Characterized Nonheme Cobalt-Hydroperoxo Complex Derived from Its Superoxo Intermediate via Hydrogen Atom Abstraction. *J. Am. Chem. Soc.* **2016**, *138*, 14186–14189.

(41) Corona, T.; Padamati, S. K.; Acuña-Parés, F.; Duboc, C.; Browne, W. R.; Company, A. Trapping of superoxido cobalt and peroxide dicobalt species formed reversibly from Co<sup>II</sup> and O<sub>2</sub>. *Chem. Commun.* **2017**, *53*, 11782–11785.

(42) Ikeda, A.; Hoshino, K.; Komatsuzaki, H.; Satoh, M.; Nakazawa, J.; Hikichi, S. O<sub>2</sub> activation and external substrate oxidation capability of a Co(II)-semiquinonato complex. *New J. Chem.* **2013**, *37*, 2377–2383.

(43) Wang, P.; Yap, G. P. A.; Riordan, C. G. Five-coordinate M<sup>II</sup>-semiquinonate (M = Fe, Mn, Co) complexes: reactivity models of the catechol dioxygenases. *Chem. Commun.* **2014**, *50*, 5871–5873.

(44) Fischer, A. A.; Lindeman, S. V.; Fiedler, A. T. Spectroscopic and computational studies of reversible O<sub>2</sub> binding by a cobalt complex of relevance to cysteine dioxygenase. *Dalton Trans* **2017**, *46*, 13229–13241.

(45) Rybak-Akimova, E. V.; Otto, W.; Deardorf, P.; Roesner, R.; Busch, D. H. Kinetics and Equilibria of Dioxygen Binding to a Vacant Site in Cobalt(II) Complexes with Pentadentate Ligands. *Inorg. Chem.* **1997**, *36*, 2746–2753.

(46) Fiammengo, R.; Bruinink, C. M.; Crego-Calama, M.; Reinhoudt, D. N. Noncovalent Secondary Interactions in Co(II)Salen Complexes: O<sub>2</sub> Binding and Catalytic Activity in Cyclohexene Oxygenation. *J. Org. Chem.* **2002**, *67*, 8552–8557.

(47) Comuzzi, C.; Melchior, A.; Polese, P.; Portanova, R.; Tolazzi, M. Cobalt(II) Dioxygen Carriers Based on Simple Diamino Ligands: Kinetic and ab Initio Studies. *Inorg. Chem.* **2003**, *42*, 8214–8222.

(48) Hu, X.; Castro-Rodriguez, I.; Meyer, K. Dioxygen Activation by a Low-Valent Cobalt Complex Employing a Flexible Tripodal N-Heterocyclic Carbene Ligand. *J. Am. Chem. Soc.* **2004**, *126*, 13464–13473.

(49) Sharma, S. K.; May, P. S.; Jones, M. B.; Lense, S.; Hardcastle, K. I.; MacBeth, C. E. Catalytic Dioxygen Activation by Co(II) Complexes Employing a Coordinatively Versatile Ligand Scaffold. *Chem. Commun.* **2011**, *47*, 1827–1829.

(50) Vad, M. S.; Johansson, F. B.; Seidler-Egdal, R. K.; McGrady, J. E.; Novikov, S. M.; Bozhevolnyi, S. I.; Bond, A. D.; McKenzie, C. J. Tuning affinity and reversibility for O<sub>2</sub> binding in dinuclear Co(II) complexes. *Dalton Trans* **2013**, *42*, 9921–9929.

(51) Blacquiere, J. M.; Pegis, M. L.; Raugei, S.; Kaminsky, W.; Forget, A.; Cook, S. A.; Taguchi, T.; Mayer, J. M. Synthesis and Reactivity of Tripodal Complexes Containing Pendant Bases. *Inorg. Chem.* **2014**, *53*, 9242–9253.

(52) Corcos, A. R.; Villanueva, O.; Walroth, R. C.; Sharma, S. K.; Bacsa, J.; Lancaster, K. M.; MacBeth, C. E.; Berry, J. F. Oxygen Activation by Co(II) and a Redox Non-Innocent Ligand: Spectroscopic Characterization of a Radical-Co(II)-Superoxide Complex with Divergent Catalytic Reactivity. *J. Am. Chem. Soc.* **2016**, *138*, 1796–1799.

(53) Anson, C. W.; Ghosh, S.; Hammes-Schiffer, S.; Stahl, S. S. Co(salophen)-Catalyzed Aerobic Oxidation of p-Hydroquinone: Mechanism and Implications for Aerobic Oxidation Catalysis. *J. Am. Chem. Soc.* **2016**, *138*, 4186–4193.

(54) Wang, Y.-H.; Pegis, M. L.; Mayer, J. M.; Stahl, S. S. Molecular Cobalt Catalysts for O<sub>2</sub> Reduction: Low-Overpotential Production of H<sub>2</sub>O<sub>2</sub> and Comparison with Iron-Based Catalysts. *J. Am. Chem. Soc.* **2017**, *139*, 16458–16461.

(55) Sharma, A. C.; Borovik, A. S. Design, Synthesis, and Characterization of Templated Metal Sites in Porous Organic Hosts: Application to Reversible Dioxygen Binding. *J. Am. Chem. Soc.* **2000**, *122*, 8946–8955.

(56) Welbes, L. L.; Borovik, A. S. Confinement of Metal Complexes within Porous Hosts: Development of Functional Materials for Gas Binding and Catalysis. *Acc. Chem. Res.* **2005**, *38*, 765–774.

(57) Lahanas, N.; Kucheryavy, P.; Lockard, J. V. Spectroscopic Evidence for Room Temperature Interaction of Molecular Oxygen with Cobalt Porphyrin Linker Sites within a Metal–Organic Framework. *Inorg. Chem.* **2016**, *55*, 10110–10113.

(58) Xiao, D. J.; Gonzalez, M. I.; Darago, L. E.; Vogiatzis, K. D.; Haldoupis, E.; Gagliardi, L.; Long, J. R. Selective, Tunable O<sub>2</sub> Binding in Cobalt(II)-Triazololate/Pyrazolate Metal–Organic Frameworks. *J. Am. Chem. Soc.* **2016**, *138*, 7161–7170.

(59) Gonzalez, M. I.; Mason, J. A.; Bloch, E. D.; Teat, S. J.; Gagnon, K. J.; Morrison, G. Y.; Queen, W. L.; Long, J. R. Structural characterization of framework–gas interactions in the metal–organic framework Co<sub>2</sub>(dobdc) by in situ single-crystal X-ray diffraction. *Chem. Sci.* **2017**, *8*, 4387–4398.

(60) Sugimoto, H.; Nagayama, T.; Maruyama, S.; Fujinami, S.; Yasuda, Y.; Suzuki, M.; Uehara, A. Thermodynamic Study on Dioxygen Binding of Diiron(II) and Dicobalt(II) Complexes Containing Various Dinucleating Ligands. *Bull. Chem. Soc. Jpn.* **1998**, *71*, 2267–2279.

(61) Li, J.; Noll, B. C.; Oliver, A. G.; Scheidt, W. R. Structural Insights into Ligand Dynamics: Correlated Oxygen and Picket Motion in Oxycobalt Picket Fence Porphyrins. *J. Am. Chem. Soc.* **2012**, *134*, 10595–10606.

(62) Friesen, B. A.; Bhattarai, A.; Mazur, U.; Hipps, K. W. Single Molecule Imaging of Oxygenation of Cobalt Octaethylporphyrin at the Solution/Solid Interface: Thermodynamics from Microscopy. *J. Am. Chem. Soc.* **2012**, *134*, 14897–14904.

(63) Hikichi, S.; Sasaki, Y.; Yoshizawa, M.; Ohzu, Y.; Moro-oka, Y.; Akita, M. Selective Synthesis, Characterization, and Configurational Flexibility of the Coordinatively Unsaturated Metal Center of Half-sandwich Type Complexes with the Less-Hindered Hydrotris-(3,5-dimethyl-4-X-1-pyrazolyl)borate Ligands [Tp<sup>Me2,X</sup>M<sup>II</sup>( $\kappa^2$ -O,O-L)] (M = Ni, Co; L = NO<sub>3</sub>, OAc; X = Me, H, Br). *Bull. Chem. Soc. Jpn.* **2002**, *75*, 1255–1262.

(64) Guzei, I. A.; Wendt, M. An improved method for the computation of ligand steric effects based on solid angles. *Dalton Trans* **2006**, 3991–3999.

(65) Calabrese, J. C.; Domaille, P. J.; Thompson, J. S.; Trofimenko, S. Steric Effects in Polypyrazolylborates: Mixed Complexes M(HB(3-isopropyl-4-bromopyrazolyl)<sub>3</sub>)L. *Inorg. Chem.* **1990**, *29*, 4429–4437.



(66) Trofimenko, S.; Calabrese, J. C.; Thompson, J. S. 1,5-Cyclooctanediybis(pyrazol-1-yl)borate: A Ligand with Enhanced Agostic Interaction. *Inorg. Chem.* **1992**, *31*, 974–979.

(67) Beugelsdijk, T. J.; Drago, R. S. Thermodynamic data for the binding of molecular oxygen to cobalt(II) protoporphyrin IX dimethyl ester. *J. Am. Chem. Soc.* **1975**, *97*, 6466–6472.

(68) El Ghomari, M. J.; Mokhlisse, R.; Laurence, C.; Le Questel, J.-Y.; Berthelot, M. Basicity of Azoles: Complexes of Diiodine with Imidazoles, Pyrazoles, and Triazoles. *J. Phys. Org. Chem.* **1997**, *10*, 669–674.

(69) *CrystalClear*; Rigaku Corporation: Tokyo, Japan, 2008.

(70) Altomare, A.; Casciaro, G.; Giacovazzo, C.; Guagliardi, A.; Burla, M. C.; Polidori, G.; Camalli, M. SIR92 - a program for automatic solution of crystal structures by direct methods. *J. Appl. Crystallogr.* **1994**, *27*, 435.

(71) Sheldrick, G. M. A short history of SHELX. *Acta Crystallogr., Sect. A: Found. Crystallogr.* **2008**, *64*, 112–122.

(72) Farrugia, L. J. WinGX suite for small-molecule single-crystal crystallography. *J. Appl. Crystallogr.* **1999**, *32*, 837–838.

(73) Farrugia, L. J. WinGX and ORTEP for Windows: an update. *J. Appl. Crystallogr.* **2012**, *45*, 849–854.